

First-principles study of structural and electronic properties of multiferroic oxide Mn_3TeO_6 under high pressure

Xiao-Long Pan(潘小龙), Hao Wang(王豪), Lei Liu(柳雷), Xiang-Rong Chen(陈向荣), and Hua-Yun Geng(耿华运)
Citation: Chin. Phys. B, 2024, 33 (**7**): 076102. DOI: 10.1088/1674-1056/ad3ef6
Journal homepage: http://cpb.iphy.ac.cn; http://iopscience.iop.org/cpb

What follows is a list of articles you may be interested in

Alloying and magnetic disordering effects on phase stability of Co_2 *Y*Ga (*Y*=Cr, V, and Ni) alloys: A first-principles study

Chun-Mei Li(李春梅), Shun-Jie Yang(杨顺杰), and Jin-Ping Zhou(周金萍)
Chin. Phys. B, 2022, 31 (**5**): 056105. DOI: 10.1088/1674-1056/ac3986

Temperature-dependent structure and magnetization of $YCrO_3$ compound

Qian Zhao(赵前), Ying-Hao Zhu(朱英浩), Si Wu(吴思), Jun-Chao Xia(夏俊超), Peng-Fei Zhou(周鹏飞), Kai-Tong Sun(孙楷橦), and Hai-Feng Li(李海峰)
Chin. Phys. B, 2022, 31 (**4**): 046101. DOI: 10.1088/1674-1056/ac2b23

Strain-tuned magnetic properties in (Ga,Fe)Sb: First-principles study

Feng-Chun Pan(潘凤春), Xue-Ling Lin(林雪玲), and Xu-Ming Wang(王旭明)
Chin. Phys. B, 2021, 30 (**9**): 096105. DOI: 10.1088/1674-1056/ac00a2

Structural modulation and physical properties of cobalt-doped layered $La_2M_5As_3O_2$ (*M*= Cu, Ni) compounds

Lei Yang(杨蕾), Yan-Peng Song(宋艳鹏), Jun-Jie Wang(王俊杰), Xu Chen(陈旭), Hui-Jing Du(杜会静), and Jian-Gang Guo(郭建刚)
Chin. Phys. B, 2021, 30 (**7**): 076106. DOI: 10.1088/1674-1056/abf349

Magnetoelectric coupling effect of polarization regulation in $BiFeO_3/LaTiO_3$ heterostructures

Chao Jin(金超), Feng-Zhu Ren(任凤竹), Wei Sun(孙伟), Jing-Yu Li(李静玉), Bing Wang(王冰), and Qin-Fen Gu(顾勤奋)
Chin. Phys. B, 2021, 30 (**7**): 076105. DOI: 10.1088/1674-1056/abf924

First-principles study of structural and electronic properties of multiferroic oxide Mn_3TeO_6 under high pressure

Xiao-Long Pan(潘小龙)[1,2], Hao Wang(王豪)[2], Lei Liu(柳雷)[2], Xiang-Rong Chen(陈向荣)[1,†], and Hua-Yun Geng(耿华运)[2,3,‡]

[1] *College of Physics, Sichuan University, Chengdu* 610065, *China*
[2] *National Key Laboratory of Shock Wave and Detonation Physics, Institute of Fluid Physics, China Academy of Engineering Physics, Mianyang* 621900, *China*
[3] *HEDPS, Center for Applied Physics and Technology, and College of Engineering, Peking University, Beijing* 100871, *China*

(Received 4 January 2024; revised manuscript received 4 April 2024; accepted manuscript online 16 April 2024)

Mn_3TeO_6 (MTO) has been experimentally found to adopt a $P2_1/n$ structure under high pressure, which exhibits a significantly smaller band gap compared to the atmospheric $R\bar{3}$ phase. In this study, we systematically investigate the magnetism, structural phase transition, and electronic properties of MTO under high pressure through first-principles calculations. Both $R\bar{3}$ and $P2_1/n$ phases of MTO are antiferromagnetic at zero temperature. The $R\bar{3}$ phase transforms to the $P2_1/n$ phase at 7.58 GPa, accompanied by a considerable volume collapse of about 6.47%. Employing the accurate method that combines DFT+U and GW, the calculated band gap of $R\bar{3}$ phase at zero pressure is very close to the experimental values, while that of the $P2_1/n$ phase is significantly overestimated. The main reason for this difference is that the experimental study incorrectly used the Kubelka–Munk plot for the indirect band gap to obtain the band gap of the $P2_1/n$ phase instead of the Kubelka–Munk plot for the direct band gap. Furthermore, our study reveals that the transition from the $R\bar{3}$ phase to the $P2_1/n$ phase is accompanied by a slight reduction in the band gap.

Keywords: magnetism, phase transition, band gap, high pressure

PACS: 61.50.Ks, 71.20.Nr, 75.50.Pp **DOI:** 10.1088/1674-1056/ad3ef6

1. Introduction

In recent years, multiferroic oxides have been extensively investigated for their potential photovoltaic applications.[1–3] As potential alternatives for the metal-halide perovskite solar cells, multiferroic oxides overcome the disadvantages (e.g., degradation, hysteresis, and lead pollutions) of traditional halide perovskites.[4–7] However, multiferroic oxides typically have wide band gaps (2.7 eV–4.0 eV)[8] that exceed the ideal value of 1.4 eV (corresponding to the maximum theoretical power conversion efficiency (PCE) for a photovoltaic material),[9] which hinders further improvement of their PCE. Therefore, reducing the band gaps of multiferroic oxides is an effective strategy to obtain materials with a high PCE. Double perovskite multiferroic oxide Bi_2CrFeO_6 has been shown to have a PCE of up to 8.1% by engineering the cationic ordering.[2] In addition, pressure, as an effective way to regulate the band gap, has been applied to the multiferroic oxide Mn_3TeO_6 (MTO).[3]

Recently, Liu *et al*. discovered that the band gap of multiferroic oxide MTO ($R\bar{3}$) was reduced by 39% (from 3.15 eV to 1.86 eV) under compression with a structural phase transition, corresponding to a transition pressure between 16 GPa and 18 GPa.[3] Such a reduction of the band gap is beneficial for applications in light-absorbing materials, which usually possess a small bandgap of about 1.4 eV. Subsequently, Arévalo-López *et al*. synthesized a novel double perovskite structure of MTO by subjecting $R\bar{3}$ crystals to high-pressure and high-temperature conditions (8 GPa and 1173 K).[10] Their research also revealed a decrease of the band gap from 2.60 eV of the $R\bar{3}$ phase to 1.80 eV of the $P2_1/n$ phase, with a reduction of 0.80 eV, and they suggest that this reduction explains the significant decrease in MTO's band gap under high pressure, as observed by Liu *et al*. At almost the same time, Su *et al*. reported that phase transition from the $R\bar{3}$ phase to the $P2_1/n$ phase in MTO occurs at the pressure of about 5 GPa based on first-principles calculations and experimental results by treating the MTO ($R\bar{3}$) crystals at 5 GPa and 1173 K.[11]

Although there is sufficient evidence in the existing studies to show that the $P2_1/n$ phase can be a high-pressure phase of the MTO, the phase transition pressure from the $R\bar{3}$ structure to the $P2_1/n$ structure reported by Su *et al*. is significantly lower than the phase transition pressure range of 16 GPa–18 GPa reported by Liu *et al*. In order to elucidate the underlying mechanism behind the significant reduction of the band gap observed in MTO, Liu *et al*. further conducted *in-situ* x-ray diffraction analysis on the structural evolution of MTO during compression and decompression processes, discovering a sequence of irreversible phase transitions: $R\bar{3} \rightarrow C2/c \rightarrow P2_1/n$.[12] Under compression, $R\bar{3}$ transforms into a $C2/c$ structure at 19 GPa, and under decompression, the $C2/c$ structure transforms into a $P2_1/n$ structure at about 9.6 GPa.

†Corresponding author. E-mail: xrchen@scu.edu.cn
‡Corresponding author. E-mail: s102genghy@caep.cn

© 2024 Chinese Physical Society and IOP Publishing Ltd

Currently, these studies have indicated that the $P2_1/n$ structure is a high-pressure phase of MTO. However, considering the differences in transition pressure from the $R\bar{3}$ phase to the $P2_1/n$ phase in previous studies, and to ascertain whether the phase with a significantly reduced band gap in MTO is indeed the $P2_1/n$ structure, further studies are needed to confirm this.

In this study, to theoretically validate the high-pressure phase transition of MTO and its associated significant reduction of the band gap, we systematically investigated the magnetic properties, phase transition, and electronic properties of MTO under high pressure through first-principles calculations. It is worth noting that compared with previous studies, we further studied the high-pressure phase transition and band gap of MTO in detail. A more accurate method combining DFT+U and G_0W_0 is used to calculate the band gap of MTO. In the next section, the computational method is formulated, the results and discussion are presented in Section 3, and Section 4 summarizes the conclusions of the paper.

2. Computational method

All first-principles calculations were performed using density functional theory (DFT)[13,14] as implemented in the Vienna *Ab initio* Simulation Package (VASP).[15,16] The description of the exchange–correlation functional adopted the Perdew–Burke–Ernzerhof (PBE)[17] generalized gradient approximation (GGA). The atomic coordinates and lattice vectors were fully optimized until the Hellmann–Feynman forces acting on each atom less than 10^{-2} eV/Å and the convergence of the total energy was better than 10^{-6} eV between two successive ionic steps. The cut-off energy for the plane-wave basis was set to 550 eV, and Monkhorst–Pack[18] k-meshes with a grid spacing of $2\pi \times 0.02$ Å^{-1} were used to sample the first irreducible Brillouin zone for all calculations, ensuring that the energy for each structure converges to 1 meV per atom. Spin polarization is taken into account in our calculations. The cell shape is completely relaxed in the calculations of structural relaxation to achieve the hydrostatic conditions. The Hubbard correction was included in the GGA+U approximation to account for strong correlation interaction between the 3d electrons of Mn atoms. Specifically, we used the simplified GGA+U method proposed by Dudarev *et al.*[19] with only a single effective U parameter. The value of U is set to 4 eV as usually adopted for Mn oxides, and we also consider some other U values for comparison in the calculations of phase transition and band gap.

In order to ensure the dynamic stability of the $R\bar{3}$ and $P2_1/n$ phases, the phonon dispersion curves were calculated using the finite displacement method implemented in ALAMODE code.[20] A $2 \times 2 \times 2$ supercell for the $R\bar{3}$ phase (160 atoms) and $1 \times 1 \times 1$ supercell for the $P2_1/n$ phase (40 atoms) were employed in the phonon spectra calculations. Given that the phonon spectrum of the $P2_1/n$ phase at zero temperature exhibits slight imaginary frequency, we calculated its phonon spectrum at high temperature by using the self-consistent phonon theory. The displacements and forces required to fit the anharmonic force constants were extracted from the snapshots obtained during *ab initio* molecular dynamics (AIMD) simulation. We conducted AIMD simulation of the $P2_1/n$ phase at 300 K using canonical ensemble, comprising a total of 4000 steps with a time step of 1.5 fs. Under equilibrium conditions, we extracted 100 sets of displacements and forces from the final 2000 steps, with an interval of 10 steps.

As is well known, the GGA exchange–correlation function tends to underestimate the band gaps of semiconductors containing 3d electrons. Therefore, it is necessary to employ a more accurate quasiparticle approximation GW approach to calculate the band gap of MTO. In our calculations, on the basis of GGA+U wave functions, G_0W_0 calculation is adopted to obtain the exact quasiparticle band structures. Wannier interpolation is used to process the calculation results of G_0W_0 to obtain quasiparticle band structures in Wannier90 software.[21]

3. Results and discussion

The four alternative phases of MTO considered in our calculations are the $R\bar{3}$ structure (existing at atmospheric conditions), the $P2_1/n$ structure (confirmed to be stable at low pressure), the Ni_3TeO_6-type $R3$ structure (common in transition metal double perovskites), and the fourth structure, the β-Li_3VF_6-type $C2/c$ structure (which was found to be a high-pressure structure of MTO[12]). As shown in Fig. 1, the $R\bar{3}$ and $R3$ phases have a triangular structure, while the $P2_1/n$ and $C2/c$ phases have a monoclinic structure. In these structures, O atoms are distributed around Mn and Te atoms to form octahedra, TeO_6 octahedra are very regular, whereas MnO_6 octahedra are considerably distorted.

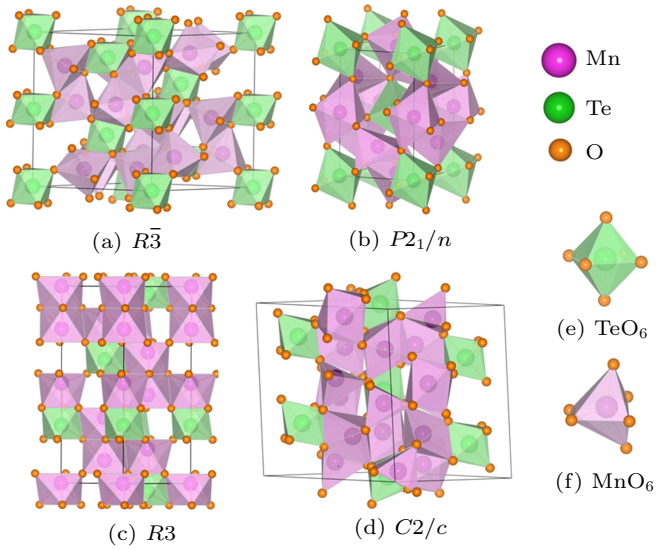


Fig. 1. Four crystal structures of Mn_3TeO_6 considered in our calculations. (a) $R\bar{3}$, (b) $P2_1/n$, (c) $R3$, and (d) $C2/c$, as well as (e) TeO_6 octahedra and (f) distorted MnO_6 octahedra.

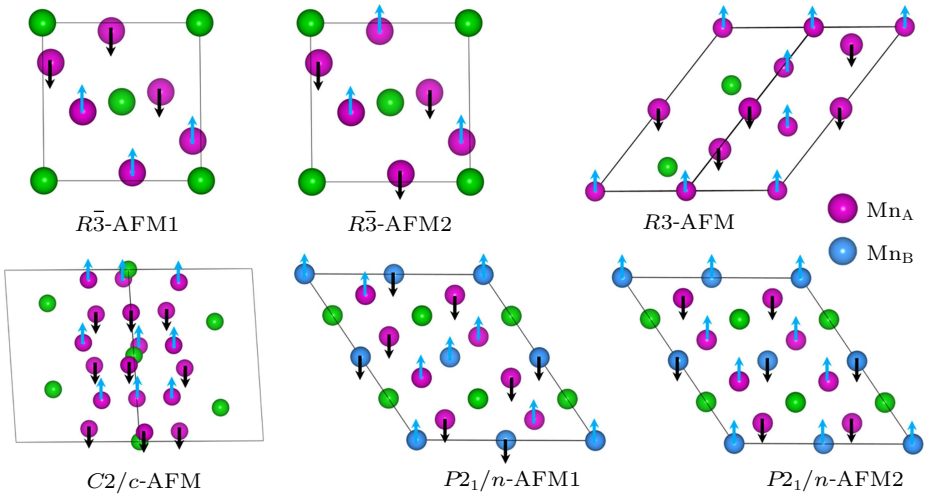


Fig. 2. Candidate antiferromagnetic ordering configurations for $R\bar{3}$, $P2_1/n$, $R3$, and $C2/c$ phases of MTO considered in our calculations. To facilitate comparison with the experimental data, the Mn atoms in the $P2_1/n$ phase can be classified into Mn_A and Mn_B atoms based on their distinct symmetries, with Mn_A occupying the 4*e* sites and Mn_B occupying the 2*b* sites of the lattice.

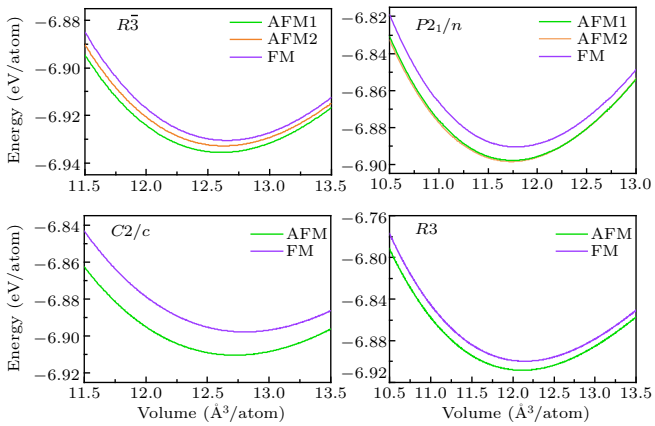


Fig. 3. Calculated energy–volume curves of the $R\bar{3}$, $P2_1/n$, $R3$, and $C2/c$ phases with different magnetic orders, respectively.

For these structures, we first compare the energy differences between different magnetic configurations to find the most stable magnetic configuration, including antiferromagnetic and ferromagnetic configurations. The candidate antiferromagnetic ordering configurations of the $R\bar{3}$, $P2_1/n$, $R3$, and $C2/c$ structures are displayed in Fig. 2. It is noteworthy that, for the $R\bar{3}$ structure, we used a rhombohedral cell with 20 atoms for magnetic calculations. For the $P2_1/n$ structure, we adopted the magnetic cell with 40 atoms proposed by Arévalo-López *et al.*, obtained using the transformation matrix: $[(1\ 0\ -1), (0\ -1\ 0), (-2\ 0\ 0)]$ with an origin shift of (0, 0, 0.5). For the $R3$ structure, we use the $1 \times 1 \times 2$ supercell of its primary cell as the magnetic structure. For the $R\bar{3}$ and $P2_1/n$ phases, we consider two antiferromagnetic configurations, while for the $R3$ and $C2/c$ phases, we only consider the simplest one. Using these magnetic configurations, we calculated the energy–volume curves for the $R\bar{3}$, $P2_1/n$, $R3$, and $C2/c$ phases, respectively, as shown in Fig. 3. We can see that the antiferromagnetic configuration is more stable than the ferromagnetic state for all phases. For $R\bar{3}$ phase, AFM1 configuration is obviously the most stable, while for $P2_1/n$, the energy of AFM1 and AFM2 orders is almost the same, with the AFM2 order slightly lower than the AFM1 order. The AFM2 configuration of the $P2_1/n$ phase obtained by our calculation is consistent with the magnetic configuration proposed by Arévalo-López *et al.*[10] Using the most stable magnetic configuration for these structures, we calculated their lattice constants at zero pressure, as illustrated in Table 1. The lattice parameters of these structures calculated in our study are in close agreement with experimental values, differing by less than 2%.

Table 1. The calculated lattice parameters of the $R\bar{3}$, $P2_1/n$, $R3$, and $C2/c$ phases by DFT+U method with $U = 4$ eV, along with previous experimental data for comparisons.

Structure	a (Å)	b (Å)	c (Å)	α (°)	β (°)	γ (°)
$R\bar{3}$ (this work)	8.94	8.94	10.77	90	90	120
$R\bar{3}$ (Su *et al.*)	8.90	8.90	10.71	90	90	120
$P2_1/n$ (this work)	5.35	5.49	7.87	90	89.77	90
$P2_1/n$ (Su *et al.*)	5.29	5.45	7.80	90	89.63	90
$P2_1/n$ (Arévalo-López *et al.*)	5.29	5.45	7.81	90	89.63	90
R3 (this work)	5.41	5.41	14.21	90	90	120
$C2/c$ (this work)	8.96	8.96	10.74	92.99	92.99	61

After obtaining the most stable magnetic configuration of each structure, we further investigate the stability of these structures under high pressure to explore the structural phase transition of MTO. The calculated enthalpy difference of the $P2_1/n$, $R3$, and $C2/c$ structures relative to the $R\bar{3}$ is shown in Fig. 4(a). The $R\bar{3}$ phase is the most stable phase in the pressure range of 0 GPa–7.58 GPa. A pressure-driven phase transition from $R\bar{3}$ phase to $P2_1/n$ phase occurs at the pressure of 7.58 GPa for MTO, consistent with the results of Su *et al.*[11] Different U values selected in the GGA+U calculations have a negligible impact on the phase transition pressure of MTO, which increases slightly with larger U values (Fig. 4(b)). Specifically, the phase transition pressure calculated with a U

value of 2 eV is only 0.13 GPa lower than the primarily used U value of 4 eV in our calculations. Above 7.58 GPa, the $P2_1/n$ phase remains stable up to 30 GPa (the maximum pressure we investigated), whereas $C2/c$ structure is energy unfavorable throughout the pressure area ($\sim$ 0.03 eV/atom higher enthalpy than the $R\bar{3}$ structure at 30 GPa). Our theoretical result is inconsistent with previous experimental study that identified a structural phase transition from $R\bar{3}$ to $C2/c$ at 19 GPa. This discrepancy may arise from the considerably lower energy barrier for the transition from $R\bar{3}$ to $C2/c$ compared to the transition from $R\bar{3}$ to $P2_1/n$, emphasizing the crucial role of kinetic effects in these transitions.[12] In addition, the $R\bar{3}$ to $P2_1/n$ transition of MTO is a typical first-order phase transition with a significant volume reduction of about 6.47%, as depicted by the equation of state (EOS) in Fig. 5. By fitting calculated EOS of the $R\bar{3}$ phase to the Vinet EOS,[22] we obtained that the volume modulus (B_0) of MTO at zero pressure is 126.16 GPa, and its pressure derivative (B') is 4.13.

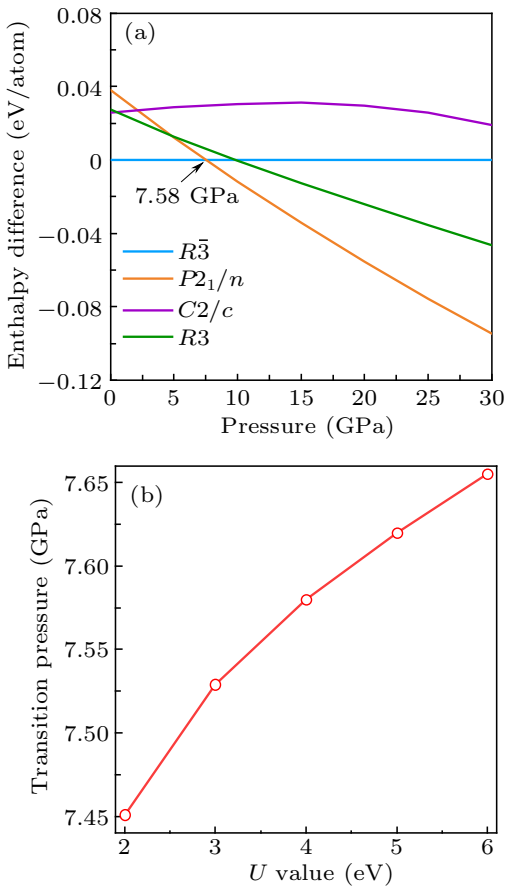


Fig. 4. (a) The calculated enthalpy difference of $P2_1/n$, $R3$, and $C2/c$ structures with respect to $R\bar{3}$ structure. (b) The change of phase transition pressure with different U values in the DFT+U calculations.

Furthermore, the calculated phonon spectra further confirm the dynamic stability of the $R\bar{3}$ and $P2_1/n$ phases at zero pressure. The phonon spectrum of the $R\bar{3}$ phase in Fig. 6(a) shows that it is dynamically stable. Given the slight imaginary frequency observed in the phonon spectrum of the $P2_1/n$ phase at zero temperature, we proceeded to calculate its phonon spectrum at 300 K using the self-consistent phonon theory, which demonstrates its dynamic stability at room temperature, as shown in Fig. 6(b).

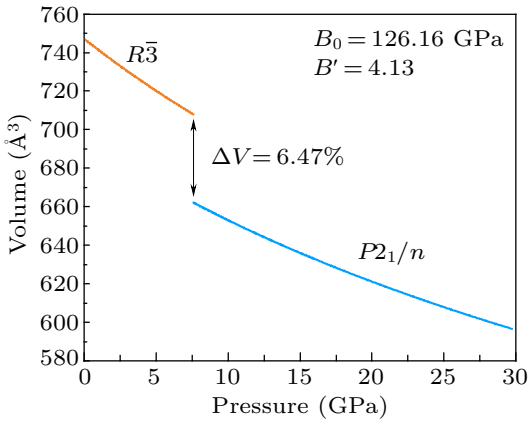


Fig. 5. Calculated equation of state (EOS) for MTO. For comparisons, the volume values of both phases are standardized to the volume corresponding to $Z = 6$.

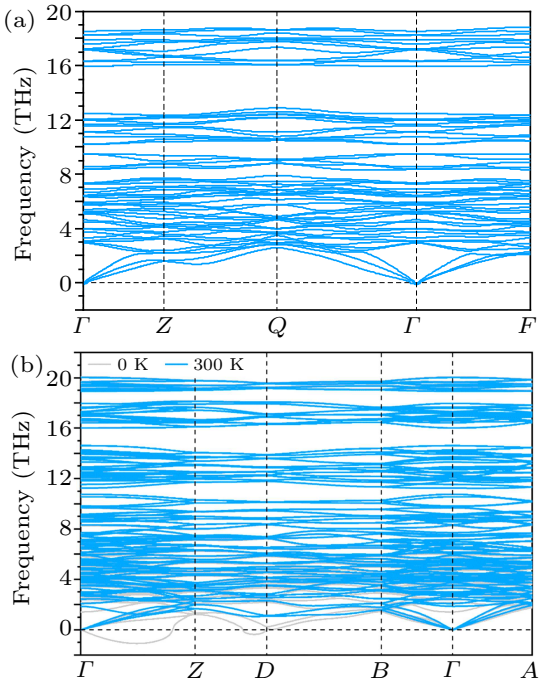


Fig. 6. The calculated phonon spectra of (a) $R\bar{3}$ and (b) $P2_1/n$ phases. For $P2_1/n$ phase, the phonon spectrum at 300 K was calculated by self-consistent phonon theory.

Next, we examine the most striking electronic properties of MTO. Results of GGA+U calculations reveal that both $R\bar{3}$ and $P2_1/n$ are semiconductors with direct band gap, and their band gap is 1.275 eV and 1.056 eV at zero pressure, respectively, as shown in Fig. 7. Note that since the spin-up and spin-down band structures for both $R\bar{3}$ and $P2_1/n$ phases are the same, we have only presented the spin-up band structures. Furthermore, pressure dependence of the band gap for MTO is illustrated in Fig. 8(a). In the stable pressure region of $R\bar{3}$ and $P2_1/n$ phases, their band gaps increase with higher pressure, and there is a decrease in the band gap by 0.197 eV (14.8%) at the phase transition pressure of 7.58 GPa. Additionally, we also investigate the relationship between the band gap of $R\bar{3}$

and $P2_1/n$ phases and the U value parameter of DFT+U calculations, with the results presented in Fig. 8(b). The band gaps of $R\bar{3}$ and $P2_1/n$ phases increase with the increased U value. When the calculations using pure GGA method or a small U value will incorrectly predict $P2_1/n$ phase to be metallic; on the contrary, a large U value (≥ 7 eV) shows that the band gaps of $R\bar{3}$ and $P2_1/n$ phases are almost equal at the phase transition pressure, which is inconsistent with the previous experimental studies. The calculated results with a U value of 4 eV show that both the band gaps and the band gap difference of the two phases are moderate, further confirming the rationality of our selected U value.

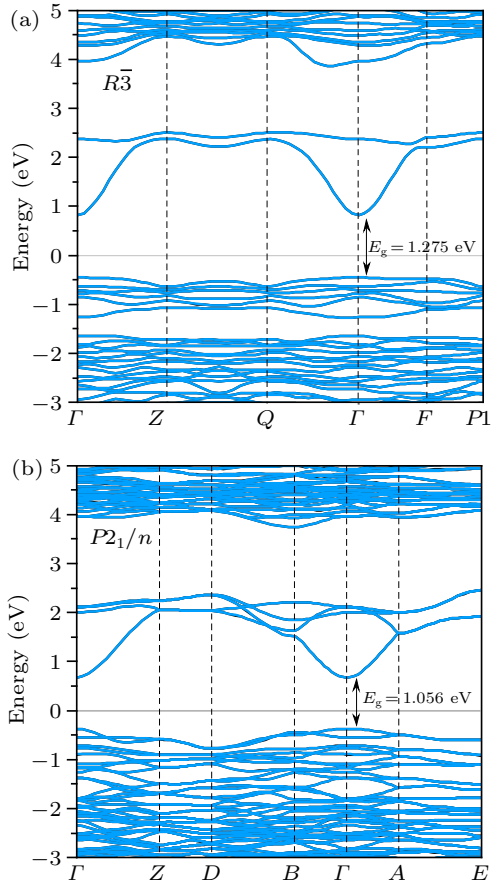


Fig. 7. Electronic band structures of the $R\bar{3}$ and $P2_1/n$ phases at zero pressure calculated by DFT+U approach.

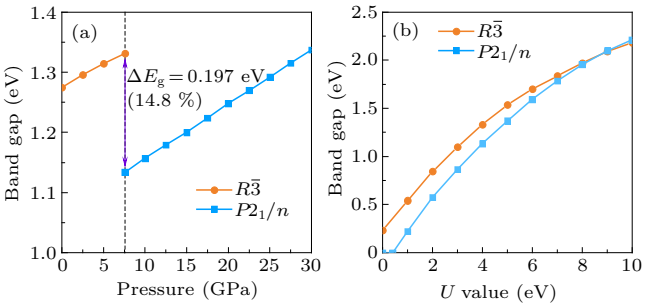


Fig. 8. (a) Pressure dependence of band gap for MTO calculated by DFT+U approach with U =4 eV. (b) Band gaps of the $R\bar{3}$ and $P2_1/n$ phases at the phase transition pressure as a function of U value.

Given that the electronic band structures calculated by GGA+U method underestimate the band gap compared to the experimental value, it is essential to employ a more accurate method to reproduce the experimental band gap of MTO. It's well known that many-body perturbation theory within the GW approximation has achieved great success in predicting the quasiparticle band structure of solid materials. Here, we combine DFT+U and G_0W_0 methods to calculate the quasiparticle band structures of MTO, and the corresponding results are shown in Fig. 9. Both $R\bar{3}$ and $P2_1/n$ phases are direct band gap semiconductor with large band gaps of 2.836 eV and 2.768 eV, respectively, and the lowest point of conduction band energy and the highest point of valence band energy are both at the gamma point. Compared with the simple GGA+U method, the band gaps calculated by G_0W_0 method have an obvious increase, with an increment of 1.561 eV for $R\bar{3}$ and 1.712 eV for $P2_1/n$. In addition, electronic projected density of states (PDOS) of MTO shows that near the Fermi level the conduction band is mainly contributed by 2p orbitals of O atoms and 5s orbitals of Te atoms for both $R\bar{3}$ and $P2_1/n$ phases, while the valence band is mainly contributed by 3d orbitals of Mn atoms and 2p orbitals of O atoms.

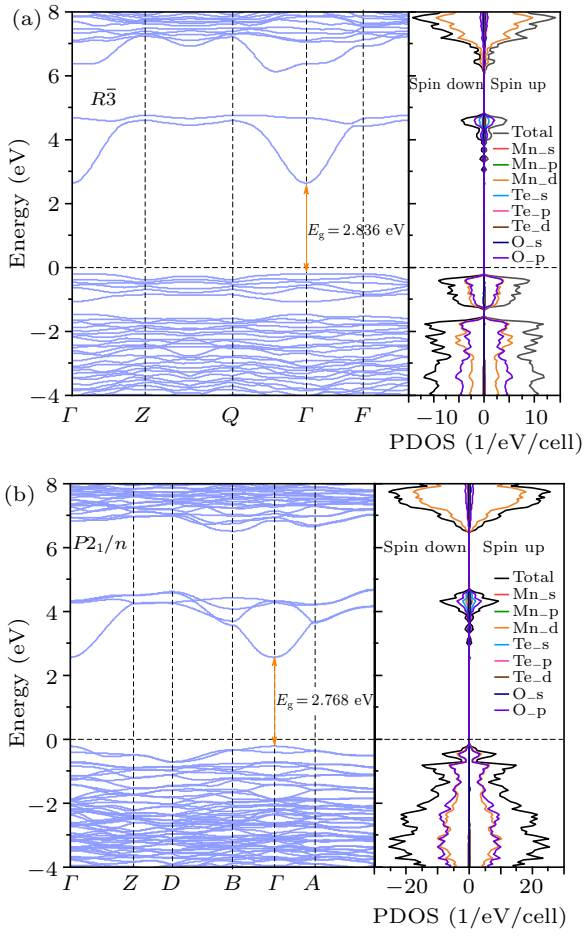


Fig. 9. The quasiparticle band structures and electronic projected density of states (PDOS) of the $R\bar{3}$ and $P2_1/n$ phases at 0 GPa calculated by combining GGA+U and G_0W_0 approach.

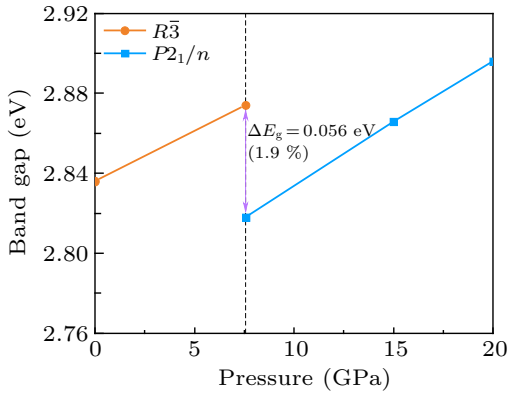


Fig. 10. Pressure dependence of band gap for MTO calculated by combining GGA+U and G_0W_0 approach.

Furthermore, the calculated band gaps of MTO under high pressure in Fig. 10 show that the band gap reduction from $R\bar{3}$ and $P2_1/n$ phases is only 0.056 eV at the phase transition pressure of 7.58 GPa, which is significantly lower than 0.8 eV observed by Arévalo-López *et al.*[10] Although the calculated band gap of 2.836 eV for the $R\bar{3}$ phase at zero pressure is close to the previously measured values of 2.6 eV by Arévalo-López *et al*. and approximately 3.05 eV by Liu *et al*., it must be acknowledged that our calculations overestimate the band gap of the $P2_1/n$ phase by about 1 eV compared to the experimental value of 1.8 eV reported by Arévalo-López *et al.*[10] The reason why our calculated band gap of the $P2_1/n$ phase is significantly higher than the experimental value reported by Arévalo-López *et al*. is that they treated the $P2_1/n$ phase as an indirect band gap semiconductor when using Kubelka–Munk plot to fit the band gap, as shown in Fig. 11(a). However, our calculations reveal that the $P2_1/n$ phase is a direct bandgap semiconductor, and Liu *et al*.'s experimental treatment[3] also categorized MTO as a direct bandgap semiconductor. According to the Kubelka–Munk formula

$$(F(R)h\nu)^{1/n} = B\left(h\nu - E_g\right),$$

where R is the reflectance, h is the Planck constant, ν is the frequency of the light, and the value of the constant n is 2 for indirect bandgap semiconductors and 1/2 for direct bandgap semiconductors, we reprocessed the experimental UV-VIS reflectance spectra data of Arévalo-López *et al*. using the formula for the direct band gap ($n = 1/2$), and the new Kubelka–Munk plot is shown in Fig. 11(b). The Kubelka–Munk plot for a direct bandgap has an obvious linear segment in the energy range of 2.75 eV–3.25 eV, and the linear fitting result shows that the band gap of the $P2_1/n$ phase is about 2.7 eV, which is very close to our calculated value. In addition, the linear segment of the Kubelka–Munk plot for a direct bandgap is more obvious than that for an indirect bandgap, which further confirms that the Kubelka–Munk plot for a direct bandgap should be adopted to obtain the band gap of the $P2_1/n$ phase. By the way, the calculated magnetic moments for Mn_A and Mn_B atoms in the $P2_1/n$ phase are 4.49 μ_B and 4.46 μ_B, respectively. While our calculated average magnetic moment per Mn atom of 4.48 μ_B matches the experimental value of 4.47 μ_B, a difference arises in the comparison with experimental values of 4.8 μ_B for Mn_A atoms and 3.8 μ_B for Mn_B atoms.[10] We further consider the effects of spin–orbit coupling (SOC) and non-collinear magnetism. The calculated results indicate that the magnitude of the magnetic moments of Mn atoms in the $P2_1/n$ phase hardly changes. Only the direction of the magnetic moment deviates slightly from the z-axis direction, with a maximum deviation angle of less than 1.5°.

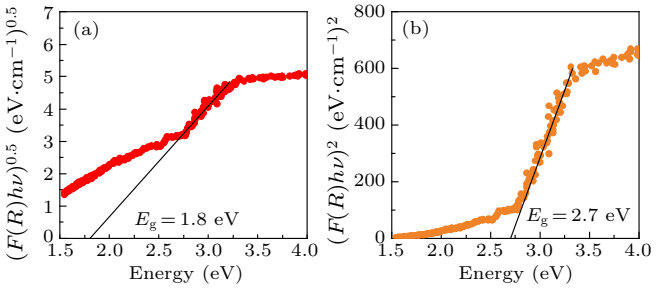


Fig. 11. Kubelka–Munk plots of the $P2_1/n$ phase for (a) an indirect band gap ($n = 2$) and (b) a direct band gap ($n = 1/2$). The corresponding UV-VIS reflectance spectra data of the $P2_1/n$ phase are extracted from Fig. 4 in the article of Arévalo-López *et al.*[10]

4. Conclusion

Through our first-principles GGA+U calculations, we determined that the antiferromagnetic configuration of the $R\bar{3}$ phase of MTO is more stable than the ferromagnetic configuration. The $P2_1/n$ phase of MTO is further confirmed to be stable under high pressure, and exhibits antiferromagnetism, consistent with previous experimental studies. At 7.58 GPa, the $R\bar{3}$ phase undergoes a first-order phase transition, transforming into the $P2_1/n$ phase, accompanied by a considerable reduction in atomic volume of about 6.47%.

The band gap of the $R\bar{3}$ phase at zero pressure, calculated using the DFT+U method, is determined to be 1.275 eV. This value is notably lower than the experimental values of 2.60 eV and 3.05 eV. Employing a more accurate method that combines DFT+U and G_0W_0, we obtained a band gap of 2.836 eV for the $R\bar{3}$ phase, which is almost consistent with the experimental values. However, our study shows that the calculated band gap (2.768 eV) of the $P2_1/n$ phase significantly overestimates the experimental value of 1.80 eV by approximately 1 eV, thereby not to theoretically predict the substantial reduction in the band gap from the $R\bar{3}$ phase to the $P2_1/n$ phase observed in previous experimental study. The reason why our theoretically calculated band gap of the $P2_1/n$ phase is significantly higher than the experimental value is that the experimental band gap was obtained using the Kubelka–Munk plot for the indirect band gap. However, the $P2_1/n$ phase is actually a direct bandgap semiconductor. Its band gap should be

determined using the Kubelka–Munk plot for the direct band gap. The band gap value of the $P2_1/n$ phase obtained by the Kubelka–Munk plot for the direct band gap is close to our calculated value. Our results also suggest that the phase transition from the $R\bar{3}$ phase to the $P2_1/n$ phase is accompanied by only a slight reduction in the band gap.

Acknowledgements

Project supported by National Key Research and Development Program of China (Grant No. 2021YFB3802300), the Natural Science Foundation of China Academy of Engineering Physics (Grant Nos. U1730248 and U1830101), and the National Natural Science Foundation of China (Grant Nos. 12202418, 11872056, 11904282, 12074274, and 12174356).

References

[1] Nechache R, Harnagea C, Licoccia S, Traversa E, Ruediger A, Pignolet A and Rosei F 2011 *Appl. Phys. Lett.* **98** 202902
[2] Nechache R, Harnagea C, Li S, Cardenas L, Huang W, Chakrabartty J and Rosei F 2015 *Nat. Photon.* **9** 61
[3] Liu L, Skogby H, Ivanov S, Weil M, Mathieu R and Lazor P 2019 *Chem. Commun.* **55** 12000
[4] Grätzel M 2014 *Nat. Mater.* **13** 838
[5] Zhang T, Chen H, Bai Y, Xiao S, Zhu L, Hu C, Xue Q and Yang S 2016 *Nano Energy* **26** 620
[6] Chen H, Zheng X, Li Q, Yang Y, Xiao S, Hu C, Bai Y, Zhang T, Wong K S and Yang S 2016 *J. Mater. Chem. A* **4** 12897
[7] Meng L, You J and Yang Y 2018 *Nat. Commun.* **9** 5265
[8] Ning C Z, Dou L and Yang P 2017 *Nat. Rev. Mater.* **2** 17070
[9] Zhang G, Wu H, Li G, Huang Q, Yang C, Huang F, Liao F and Lin J 2013 *Sci. Rep.* **3** 1265
[10] Arévalo-López Á M, Solana-Madruga E, Aguilar-Maldonado C, Ritter C, Mentré O and Attfield J P 2019 *Chem. Commun.* **55** 14470
[11] Su H P, Li S F, Han Y F, Wu M X, Gui C R, Chang Y F, Croft M, Ehrlich S, Khalid S, Adem U, Dong S, Sun Y, Huang F and Li M R 2019 *J. Mater. Chem. C* **7** 12306
[12] Liu L, Geng H Y, Pan X, Song H X, Ivanov S, Mathieu R, Weil M, Li Y, Li X and Lazor P 2022 *Appl. Phys. Lett.* **121** 044102
[13] Hohenberg P and Kohn W 1964 *Phys. Rev.* **136** B864
[14] Kohn W and Sham L J 1965 *Phys. Rev.* **140** A1133
[15] Kresse G and Hafner J 1993 *Phys. Rev. B* **47** 558
[16] Kresse G and Furthmuller J 1996 *Comput. Mater. Sci.* **6** 15
[17] Perdew J P, Burke K and Ernzerhof M 1996 *Phys. Rev. Lett.* **77** 3865
[18] Monkhorst H J and Pack J D 1976 *Phys. Rev. B* **13** 5188
[19] Dudarev S L, Botton G A, Savrasov S Y, Humphreys C J and Sutton A P 1998 *Phys. Rev. B* **57** 1505
[20] Tadano T and Tsuneyuki S 2015 *Phys. Rev. B* **92** 054301
[21] Mostofi A A, Yates J R, Lee Y S, Souza I, Vanderbilt D and Marzari N 2008 *Comput. Phys. Commun.* **178** 685
[22] Vinet P, Ferrante J, Rose J H and Smith J R 1987 *J. Geophys. Res.* **92** 9319